Asociación Argentina
de Mecánica Computacional

Mecánica Computacional Vol XXXV, págs. 567-594 (artículo completo)
Martín I. Idiart, Ana E. Scarabino y Mario A. Storti (Eds.)
La Plata, 7-10 Noviembre 2017

NONLINEAR VISCOUS DAMPING AND TUNED MASS DAMPER DESIGN FOR OCCUPANT COMFORT IN FLEXIBLE TALL BUILDINGS SUBJECTED TO WIND LOADING

José A. Inaudi[a,b], Michael Rendel[c] and Ignacio Vial[c]

[a]*Departamento de Aeronáutica, Facultad de Ciencias Exactas, Físicas y Naturales, Universidad Nacional de Córdoba, Av. Velez Sársfield 1611, 5000 Córdoba, Argentina*
http://www. www.efn.uncor.edu

[b]*SIRVE Argentina, Córdoba, Argentina*
inaudijose@gmail.com

[c]*SIRVE Engineering Consulting*
Av. Presidente Riesco 5435, Las Condes, Santiago de Chile,
http://www.sirve.cl

Keywords: wind, vibration, damping, random processes, statistical linearization, structural dynamics

Abstract. During wind events, tall buildings may exhibit floor accelerations levels that compromise occupant comfort. The use of energy dissipating devices to reduce peak floor accelerations is a sound strategy to improve building performance. The estimation of mean peak floor accelerations of a steel-frame building subjected to random wind forces and the design procedure of supplemental nonlinear viscous dampers to improve occupant comfort in one-year recurrence wind events are described in this paper. A stochastic wind load model is developed to estimate acceleration performance; drag, lift and torsional moments at each story are defined as random stationary processes by the definition of their cross-spectral density matrix. Wind tunnel results and computational fluid dynamic analyses are used to fine-tune the stochastic load models. Reduced-order structural models of the tower are developed to estimate the frequency response function from floor loadings to floor accelerations at corners points of the buildings. Statistical linearization is used to estimate the performance of the buildings with non-linear viscous dampers installed in different configurations. Floor acceleration reductions achieved with supplemental viscous dampers and a tuned mass damper are evaluated to comply with occupant performance standards.

1 INTRODUCTION

Flexible tall towers are sensible to wind action, suffering vibrations during wind events due to dynamic loading caused by random pressures imposed by turbulent air in motion (buffeting) and vortex shedding. Stochastic building wind-force models have been developed with theoretical and wind tunnel model testing by several authors (Kareem, 1992). Turbulence intensity profile of the atmospheric boundary layer is relatively high in urban areas and reduces with height. Longitudinal turbulence can be modelled as a broad-band stochastic process; Kaimal and Von Karman spectra are typical power spectral densities used for turbulence modelling (Kareem, 1992; Tamura and Kareem, 2013).

Experimental studies on occupant comfort have led to different standards for assessing total peak acceleration thresholds that guarantee comfort under serviceability conditions, such as one-year recurrence wind events (Tamura and Kareem, 2013; ISO 10137, 2007). In tall flexible lightly-damped structures, reaching these standards often requires supplemental damping devices connected to the structure such as: viscoelastic, viscous, friction dampers, tuned mass dampers (TMD) or tuned liquid dampers, among other protective strategies.

This paper presents a methodology for performance assessment of flexible buildings subjected to wind induced vibrations and nonlinear damper design strategies for performance improvement applications in a specific tower project to be built in Auckland, New Zealand, part of a consultancy project developed by the authors. Section 2 describes the dynamic characteristics of the building and desired wind performance. Section 3 is devoted to the damping design strategy for the tower; nonlinear viscous dampers are the selected design alternative in this case. In this section the analysis procedure for performance assessment of the structure without and with nonlinear damper devices is presented. A stochastic wind load model in combination with the statistical linearization method is used for damper parameter definition and performance assessment for different damper configurations. Section 4 reports the expected performance improvements of the building with additional nonlinear viscous dampers and with dampers and a TMD. Concluding remarks are presented in Section 5.

2 DYNAMIC CHARACTERISTICS OF THE TOWER UNDER STUDY

2.1 Customs Tower in Auckland

The project that motivated this study is a new building of approximately 200 meters in height, comprising 50 levels above ground and 5 basement levels below ground (see Fig 1). Peddle Thorp Group is responsible for the architecture of the project and Mott MacDonald leads the engineering team. Windtech Consultants developed the wind engineering, wind tunnel studies and load cases used for structural design verification and rms (root mean square) and PSD (power spectral density) of base moments used for wind-force model adjustment. The authors and SIRVE Chile developed the wind model and damper design strategy reported herein.

The tower is mainly residential and has 2 parking levels above ground and some office and retail accommodation on the lower floors.

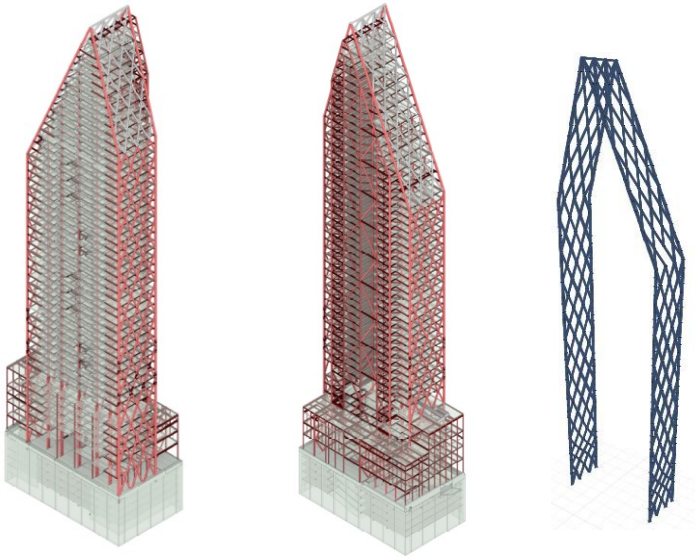

Figure 1. 3D view of the Revit Structural model (provided by Mott MacDonald)
North East view (left), South West view (center) and external braced mega-frame (right)

The basement structure (Ground and underground levels B_1 to B_5) will be constructed predominantly with reinforced concrete and the superstructure with a combination of steel moment resisting frames and braced frames. An external steel braced mega-frame (Fig.1) connected to the main structure every 2 stories provides significant stiffness in the *Y* direction of the building. Because diagonal bracings frames acting in the X direction are concentrated mainly on one side of the building structure there is an important lateral-torsional coupling in the *X*-direction vibration mode. As shown in Figure 2, the natural periods of vibration of the first two modes of the structure are above 4 seconds.

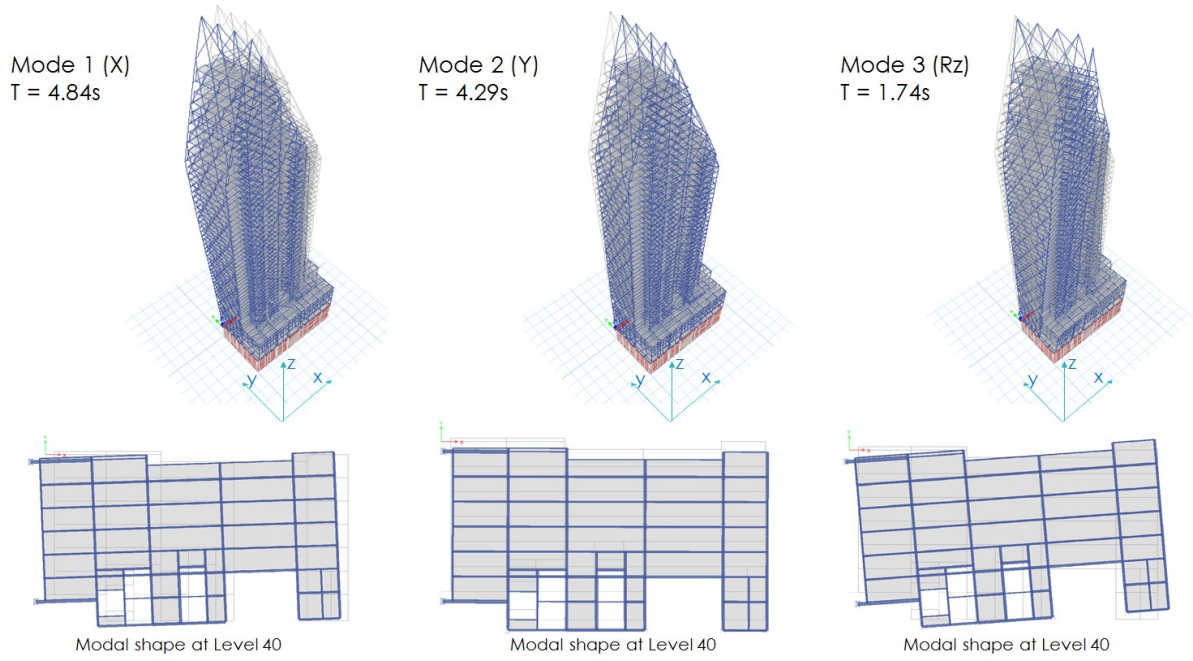

Figure 2. First three mode shapes and natural periods of vibration (original structure)

2.2 Desired Performance

The main objective of the consultancy work was to design a vibration control system for the tower to achieve the performance required according by the following human comfort criteria:

Table 1. Human comfort criterion for OCC

Type	Criterion	Maximum Value
1 year return period peak total floor acceleration	W.H. Melbourne (1988)	10.2 milli g
1 year return period peak total floor acceleration	ISO 10137 (2007) for residential towers	7.7 milli g
1 year return period peak rotational velocity	Isyumov (1993)	1.5 milli rad/s

Other important aspects taken in consideration were: i) Compliance with the current architectural layout), ii) Cost effective solution, and iii) Effectiveness for serviceability and ultimate states: (provide reduction of vibrations for serviceability states (human comfort) and ensure integrity for ultimate conditions: (a) 1,000 years return period wind loads, and (b) maximum earthquake loads).

3 DYNAMIC MODELING AND ANALYSIS OF THE TOWER WITH DAMPERS

3.1 Damping augmentation strategy

Preliminary studies of the building developed by Windtech Consultants (Windtech 2016) indicated that modal damping ratios of the tower should be augmented from values of the order of 1% to 3% or more in the first three modes of vibration to comply with occupant comfort criteria for one-year return period wind condition. No specific recommendations were done for high-intensity wind events, indicating that modal damping increase for high-intensity events was not necessary for structural safety. Because modal damping ratio increase was the main objective for the dissipation system, viscous dampers were preferred by the authors over viscoelastic devices to provide larger energy dissipation for a given level of peak damper force.

In the case the desired performance could not be reached with viscous dampers, due to location limitations defined by the architects and structural limitations for damping augmentation due to interaction of viscous damper and elastic steel members, an additional TMD could be considered to improve performance.

The proposed strategy to increase energy dissipation capacity, was then to include nonlinear viscous dampers with constitutive relations of the form

$$f_{vd} = c\,|\dot{\Delta}|^{\alpha}\,\text{sign}(\dot{\Delta}) \tag{1}$$

where:

f_{vd}: Force of the device as response to the damper deformation velocity $[kN]$
c: Viscous damping constant $[kN(s/m)^{\alpha}]$

$\dot{\Delta}$: Damper deformation velocity $[m/s]$
α: Velocity exponent (typically in a range from 0.3 to 2.0)

The main advantages of low α exponents (< 0.5) over linear viscous damping (α =1) are:

- Small α exponents (0.3, for example) provide higher energy dissipation for low intensity winds compared to linear viscous dampers.
- Small α exponents provide reduced damper forces for 10^3 year return period wind and earthquake loads compared to linear viscous dampers, reducing the cost of diagonal bracing required to connect the dampers to the main structural system.

3.2 Structural Analysis Methodology for Damping Parameter Optimization

The process of damper configuration design and damper parameter definition required the development of an analysis methodology and a piece of software that could estimate stochastic performance of the structure for one-year return period wind events, given the nonlinear constitutive relation of the viscous dampers are described in this section.

A cost-performance optimization was carried out comparing different dissipation configurations. Performance was measured in terms of modal damping increase and acceleration performance for OCC defined for 1-year recurrence wind events. Stochastic analyses of a linear equivalent structural model were performed with non-linear distributed dampers, using statistical linearization techniques and a stochastic wind load model. A reduced order model of the structural system was developed exporting, from ETABS® structural model, 200 mode-shape vectors computed using load-dependent Ritz vectors associated to forces on elastic bracings connecting each damper to the main structure for each damper configuration analyzed. The applied methodology is conceptually depicted in Figure 3 with the responsible party (JAI: José A. Inaudi, SIRVE Consulting, Wintech Consulting and Mott MacDonald).

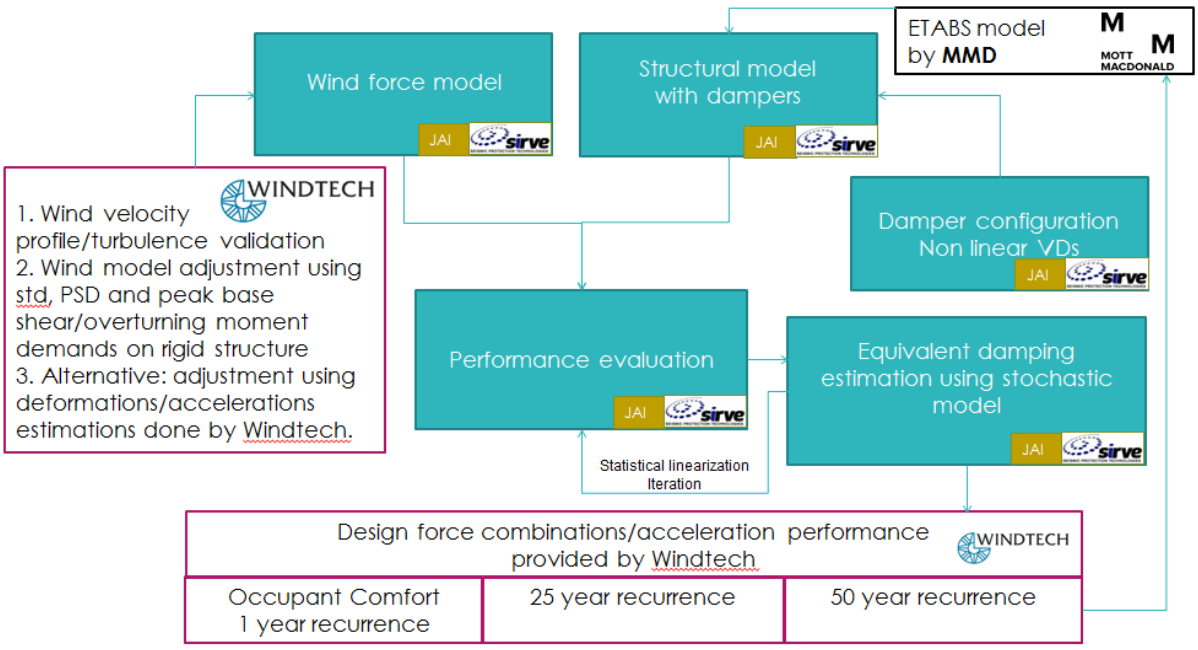

Figure 3. Conceptual representation of the methodology for damper design.

As result of this design stage, a damper configuration was selected to develop a preliminary construction budget, previous to the detailed engineering design stage.

3.3 Proposed damper locations and toggle connections

Several arrangements of dampers were proposed for evaluation in coordination with the structural engineer and the architect of the project. Those that best fit with the architectural and structural design of the building and were selected for analysis are the following:

I. 64 VDs: 64 viscous dampers on diagonal braces located on GLs 2 and 6 between GLs D and F

II. 36 VDs: 28 viscous dampers on toggle braces + 8 viscous dampers on diagonal braces, located on GLs 2 and 6 between GLs D and F

III. 60 VDs: Configuration II + 10 viscous dampers on toggle braces + 14 viscous dampers on diagonal braces, located on GL 4 between GLs D and F

IV. 54 VDs: Configuration II + 18 VDs on toggle braces, located on GL D between GLs 2 and 3

V. 73 VDs: Configuration III + 13 VDs on toggle braces, located on GL D between GLs 4 and 5

VI. 36VDs + TMD: Configuration II + 150 Ton Tuned Mass Damper (TMD)

Figures 4 and 6 show configuration II and VI studied, which were the selected configurations for future construction (with some modifications commented later). Elevation views of these additional configurations are not shown for brevity. Deformation rate exponents were selected as $\alpha = 0.3$ for toggle dampers and $\alpha = 0.5$ for dampers connected by diagonals.

Arrangement II: 36 viscous dampers. Configuration description:

- Gridline 2: 14 viscous dampers on toggle braces + 8 viscous dampers on diagonal braces, all between gridlines D and F
- Gridline 6: 14 viscous dampers on toggle braces between gridlines D and F
- Total number of dampers: 36 on gridlines 2+6

Arrangement VI: 36 viscous dampers along GLs 2 and 6, + 150 Ton TMD. Configuration description

- Gridline 2: 14 viscous dampers on toggle braces + 8 viscous dampers on diagonal braces, all between gridlines D and F
- Gridline 6: 14 viscous dampers on toggle braces between gridlines D and F
- Level 55: 150 Ton TMD
- Total number of dampers: 36 viscous dampers + TMD (grid lines 2+6 & Level 55)

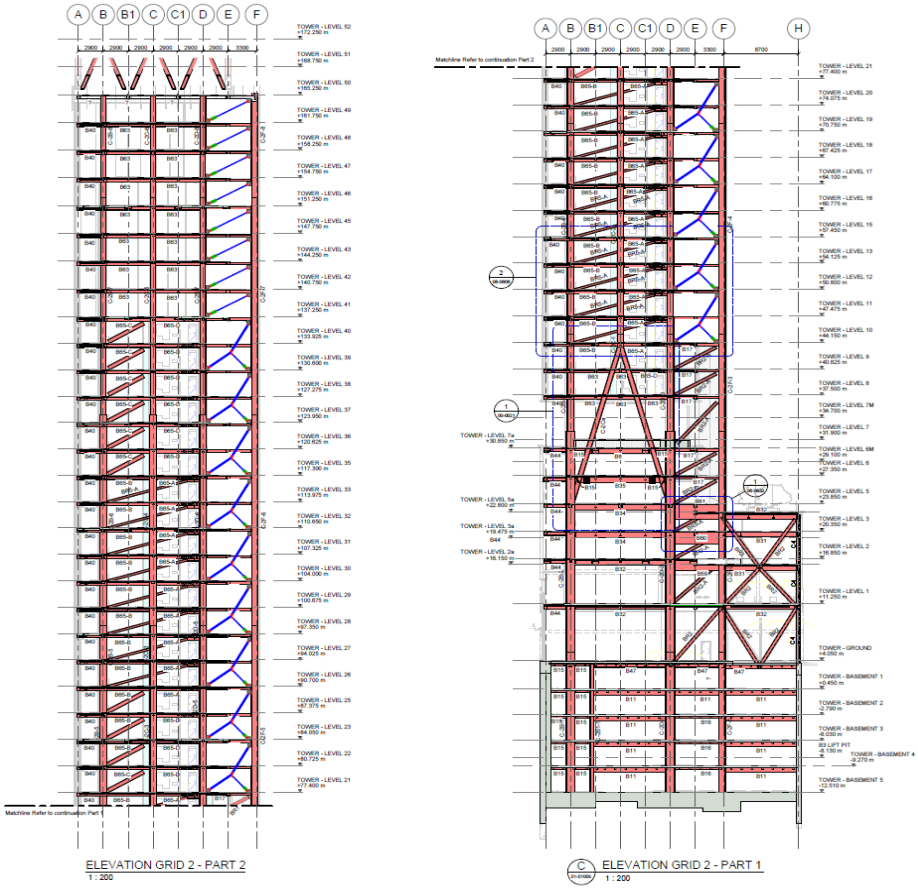

Figure 4. Gridline 2 elevation view for Arrangement II - Damper braces in blue lines

Extracted and modified from WIP Structural Project Plans (Mott MacDonald)

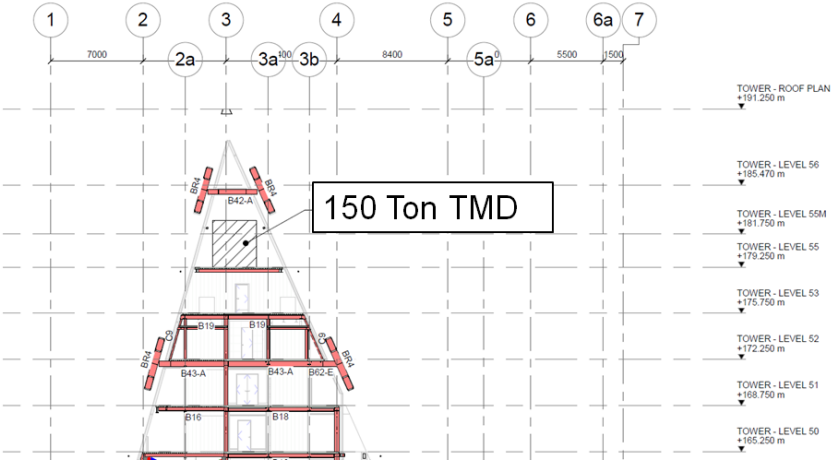

Figure 5. Upper floors elevation view for Arrangement VI – TMD location

As shown in Figure 5 arrangement VI included a linear TMD of 150 metric tons located at the top of the building with tuning and damping parameters optimized so as to minimize total peak acceleration at L52.

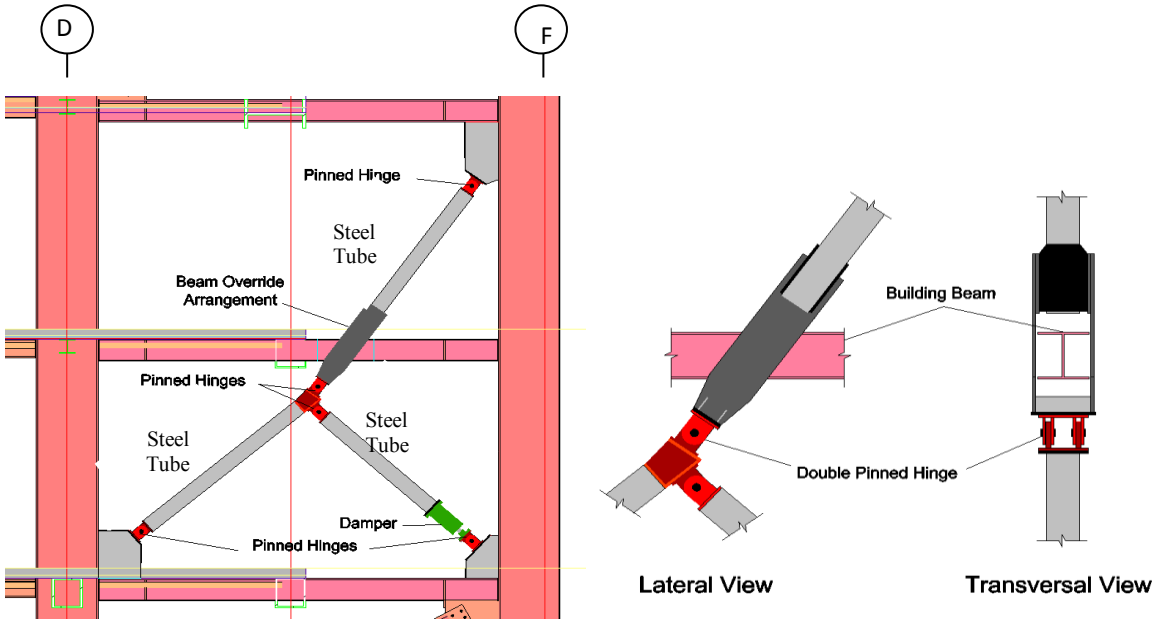

Figure 6. Typical toggle brace and damper connectivity layout and beam override arrangement

Relative displacements in the toggle connections between connected floors are small (≈ 0.35 mm to 0.6 mm RMS) for OCC loads. Displacements in this range require special types of viscous dampers and the system might be vulnerable to other efficiency losses. As the deformations on dampers are small, any loss in elastic deformations and gaps might generate an inefficient performance.

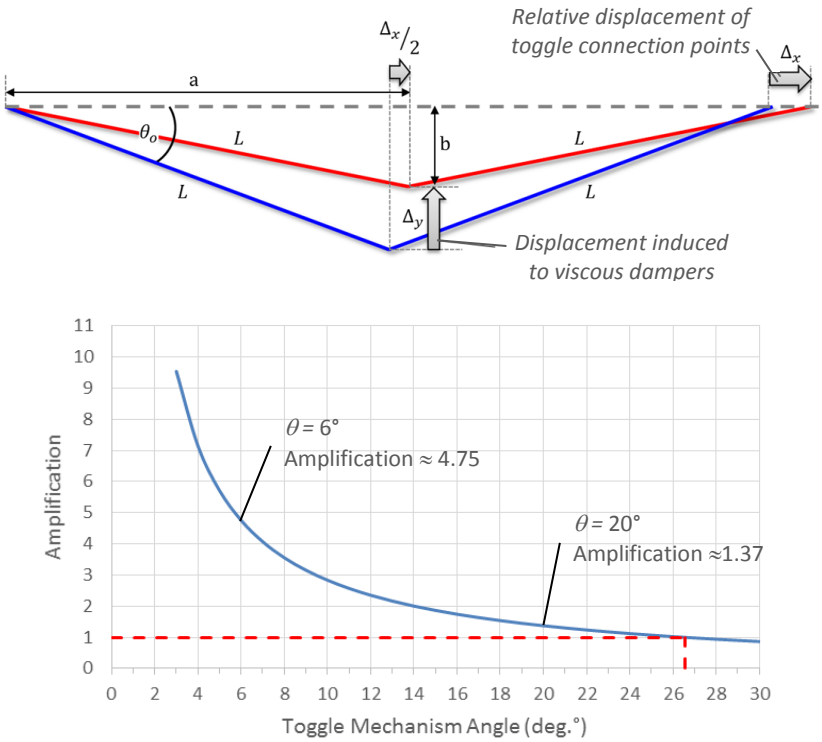

Figure 7. Toggle mechanism kinematics and displacement amplification as function of toggle braces angle.

Toggle mechanisms can increase damper deformations by about 5 times, making them work at more conventional stroke levels and smaller forces. Both of these effects lead to more cost effective devices. This consideration dictated alternative arrangements considering the use of toggle braces connecting two consecutive stories to increase damper deformations and deformation rates, as shown in Figure 6; the toggle connection design needs to consider a system to override the structural elements at the mid-story as shown.

The kinematics of the toggle mechanism and the relative displacement amplification, ratio of relative displacements Δ_y/Δ_x (see Fig. 7), as a function of the initial angle θ_o of the axially rigid braces are shown in Figure 6. We notice that displacement amplification $\Delta_y/\Delta_x > 1$ is achieved for any brace angle $\theta_o < 26.5°$ and it increases for smaller angles. For $\theta_o = 6°$, amplification of the order of 4.75 is achieved.

3.4 Stochastic Wind Load Model

A stochastic model for along the wind, across the wind and torsional moments acting at each level of the structure was developed using theoretical formulations available in the literature. The main characteristics of the wind load model developed for this project are the following:

- Random characterization of wind turbulence
- Includes spatial coherence of wind forces through spatial coherence functions of wind turbulence
- Represents stationary demand along the wind, across the wind and torsional effects of wind pressures
- The model uses wind information based on wind tunnel tests (provided by Windtech)
- The stochastic load model provides also artificial wind load signals for validation with a nonlinear response using conventional structural software (ETABS).

The inputs required for the stochastic model are:

- $U(z)$ mean wind profiles for different wind directions and wind recurrence period provided by Windtech
- $I_t(z)$ turbulence intensities for different wind directions and wind recurrence periods as function of height z.
- Integral length scale $L_t(z)$ for Von Karman PSD spectrum of longitudinal turbulence
- Base moments (overturning X and Y, and torsional Z) and base shear RMS and PSD demand from wind tunnel tests by Windtech for model adjustment
- Spatial correlation of longitudinal turbulence
- Admittance function

The stochastic load model for X and Y wind direction assumes statistical independence of along the wind, $\boldsymbol{F}_D$, across the wind forces $\boldsymbol{F}_L$, and $\boldsymbol{M}_z$ torsional moments applied at each level of the structure. The model is defined in the frequency domain by the corresponding cross PSD matrices for the along-the-wind force vector, $\boldsymbol{S}_{\boldsymbol{F}_D\boldsymbol{F}_D}(f)$, across-the-wind force vector, $\boldsymbol{S}_{\boldsymbol{F}_L\boldsymbol{F}_L}(f)$, and the torsional moment vector, $\boldsymbol{S}_{\boldsymbol{M}_z\boldsymbol{M}_z}(f)$, as functions of frequency f (in

Hertz). Base moments rms and PSDs were used to fit parameters of the stochastic force model.

Along the wind forces PSD matrix was estimated using longitudinal turbulence intensity profile, mean wind profile, an admittance function, a space-correlation turbulence model in height and the estimated drag coefficient distribution. The along-the-wind (drag) coefficient profile as a function of height z and wind angle, was estimated by a Computational Fluid Dynamics (CFD) RANS[1] analysis considering the detailed geometry of the building (Fig. 8).

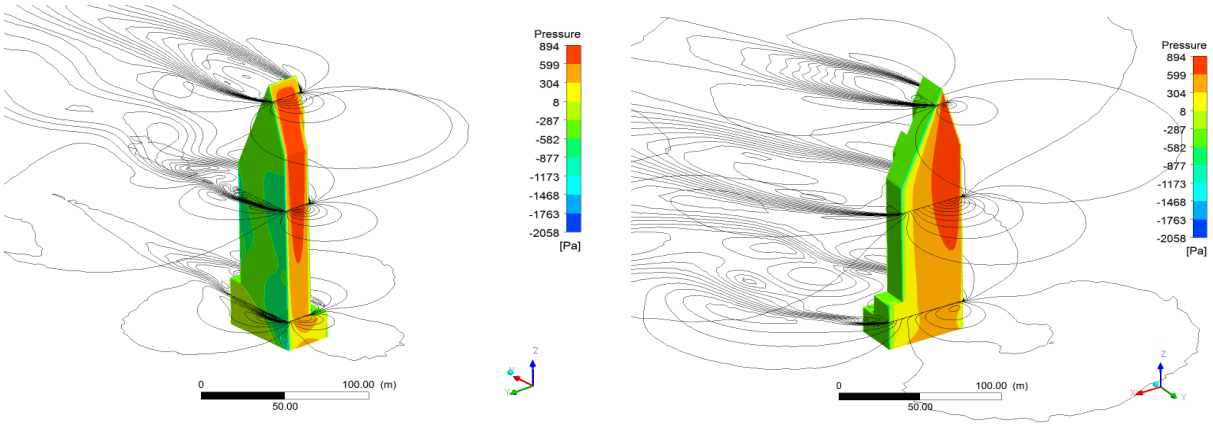

X direction Analysis Y Direction Analysis

Figure 8. CFD Rans Analysis for determination of along the wind force coefficient as function of height

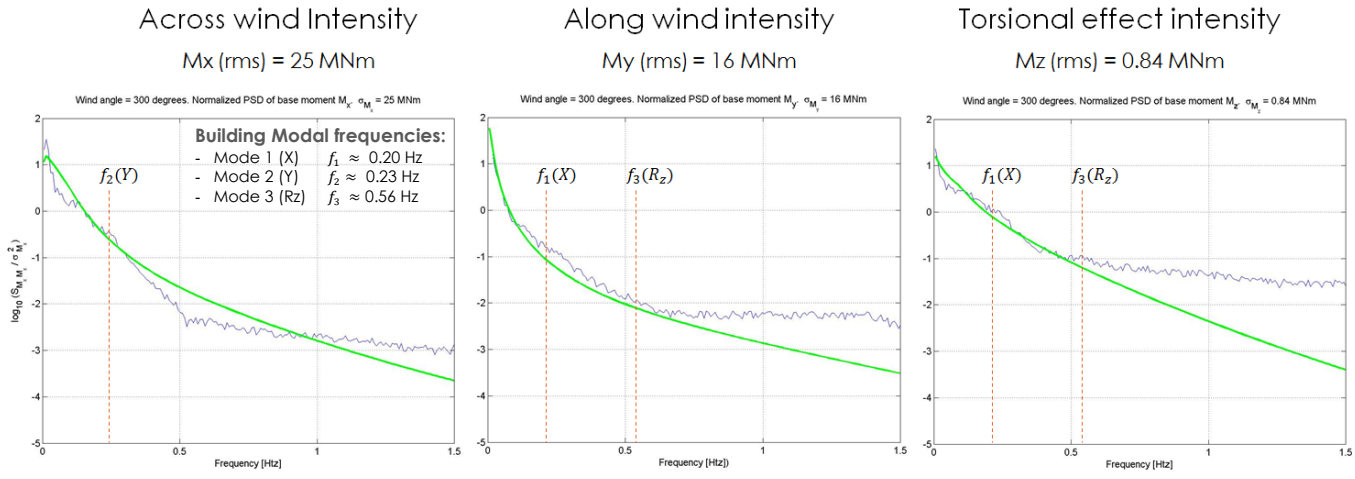

Figure 9a. PSD and total Intensity of the base moment for wind acting in the ***X*** direction. Wind test experimental results (blue) and theoretical model (green)

[1] CFD Analysis solving Reynolds-averaged Navier-Stokes equations.

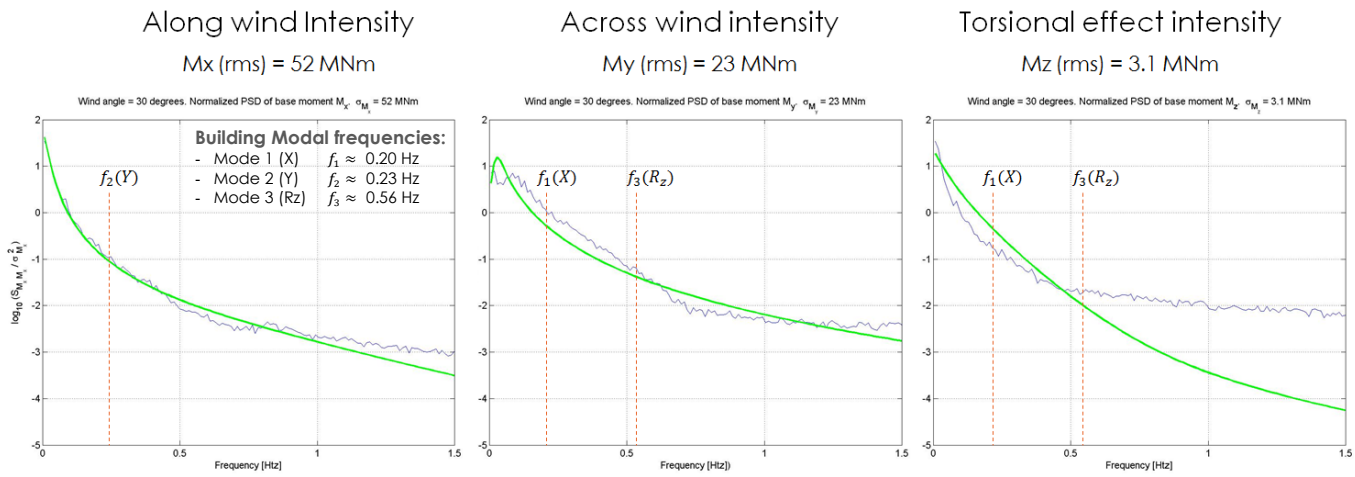

Figure 9b. PSD and total Intensity of the base moment for wind acting in the ***Y*** direction. Wind test experimental results (blue) and theoretical model (green)

The stochastic wind-force model was checked and adjusted computing the PSDs of the base moments of the model and comparing them with experimental rms and PSDs of base moments in X, Y and Z directions to enforce the same rms base moments as those reported by Windtech based on wind tunnel testing in each wind direction considered. The result of this adjustment for the X and Y Wind directions is presented in Figures 9a and 9b, where the thin blue line is the experimental result PSD in $\log_{10}$ scale, and the thick green line is the PSD of the theoretical wind model. Main building modal frequencies are shown in the figures as reference values.

3.5 Performance estimation using stochastic wind load and statistical linearization

The general process for developing the probabilistic analysis and obtaining equivalent modal damping and performance results is shown in Figure 10. The analysis requires an iteration process because $c_{d,i}^{eq}$ of each damper depends on the assumed rms deformation rates of the dampers that in turn depend on the equivalent damping matrix of the model.

The dynamic model of the structure with nonlinear viscous damper can be expressed

$$\boldsymbol{M}\ddot{\boldsymbol{q}}(t) + \boldsymbol{C}\dot{\boldsymbol{q}}(t) + \boldsymbol{K}\boldsymbol{q}(t) + \sum_{i=1}^{N_d} \boldsymbol{L}_i^T c_i |\boldsymbol{L}_i \dot{\boldsymbol{q}}(t)|^{\alpha} \text{sign}(\boldsymbol{L}_i \dot{\boldsymbol{q}}(t)) = \boldsymbol{L}_{\boldsymbol{qw}} \boldsymbol{w}(t) \qquad (2)$$

Diagonal matrices $\boldsymbol{M}$ and $\boldsymbol{K}$ are defined for the modal coordinates $\boldsymbol{q}(t)$ of the reduced order model (200 Ritz modal coordinates). $\boldsymbol{L}_\text{i}$ is the kinematic transformation from modal coordinates to the i-th damper deformation,

$$\Delta_i(\text{t}) = \boldsymbol{L}_\text{i}\boldsymbol{q}(t) \qquad (3)$$

$\boldsymbol{L}_{\boldsymbol{qw}}$ is the wind force influence vector from wind loads to generalized forces in modal coordinates, and $\boldsymbol{w}(t)$ is the wind force vector composed by along the wind, across the wind and torsional moments for each level

$$\boldsymbol{w}(t)^T = [\boldsymbol{F}_D^T \ \boldsymbol{F}_L^T \ \boldsymbol{M}_z^T \ ] \qquad (4)$$

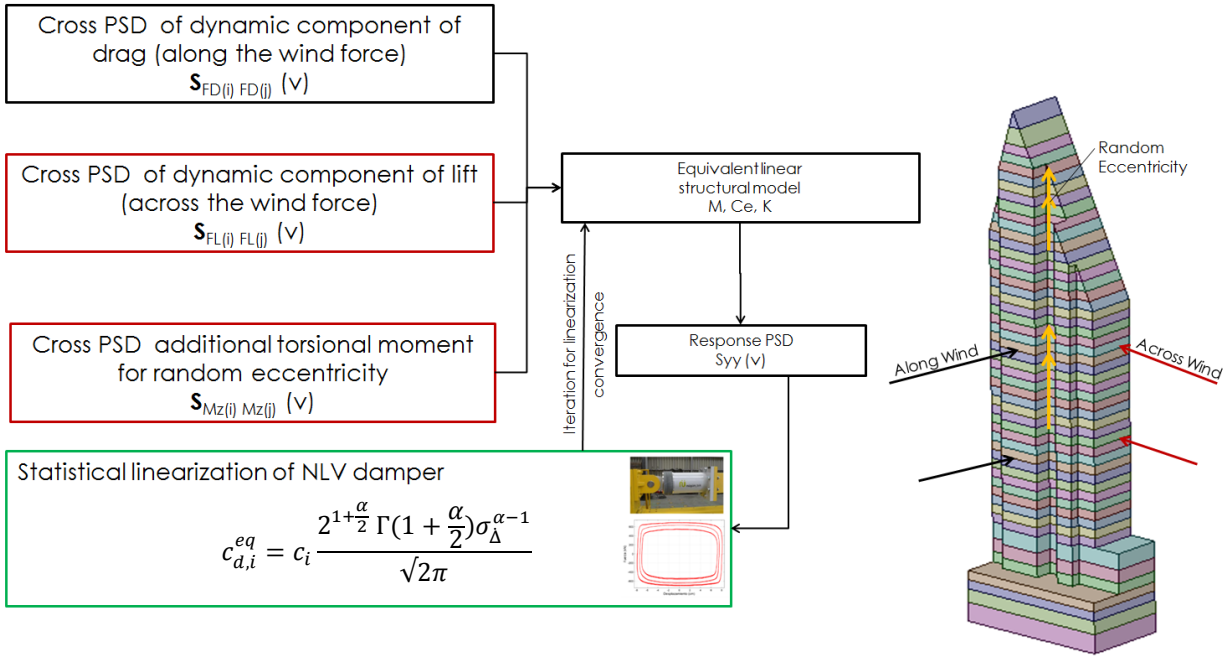

Figure 10. Summarized flowchart for probabilistic wind analyses in the Y direction of the building

For a stationary input vector signal $\boldsymbol{w}(t)$, an estimation of the stationary response of the model can be obtained using an equivalent linear model assembling the equivalent damping matrix of the nonlinear viscous dampers, to yield

$$\boldsymbol{M}\ddot{\boldsymbol{q}}(t) + \boldsymbol{C_e}\dot{\boldsymbol{q}}(t) + \boldsymbol{K}\boldsymbol{q}(t) = \boldsymbol{L_{qw}}\boldsymbol{w}(t) \tag{5}$$

where damping matrix $\boldsymbol{C_e}$ is computed summing the diagonal modal damping matrix (with modal damping ratios of 0.01) and the contribution of the equivalent damping parameters of the nonlinear dampers

$$\boldsymbol{C_e} = \boldsymbol{C} + \sum_{i=1}^{N_d} \boldsymbol{L}_i^T c_{d,i}^{eq} \boldsymbol{L}_i \tag{6}$$

$$c_{d,i}^{eq} = c_i \frac{2^{1+\frac{\alpha}{2}}\Gamma(1+\frac{\alpha}{2})\sigma_{\dot{\Delta}_i}^{\alpha-1}}{\sqrt{2\pi}} \tag{7}$$

Mean square deformation rates of the dampers can be expressed as

$$\sigma_{\dot{\Delta}_i}^2 = \boldsymbol{L}_i E[\dot{\boldsymbol{q}}\dot{\boldsymbol{q}}^T]\boldsymbol{L}_i^T \tag{8}$$

The computation of the one-sided PSD matrix $\boldsymbol{S_{yy}}(f)$ is done using the frequency response function from wind force vector $\boldsymbol{w}^T = [\boldsymbol{F_D^T}\ \boldsymbol{F_L^T}\ \boldsymbol{M_z^T}]$ to any output vector $\boldsymbol{y}(t)$ of interest, using standard random vibration analysis in the frequency domain

$$S_{yy}(f) = \boldsymbol{H_{yw}}(f)^* \boldsymbol{S_{ww}}(f) \boldsymbol{H_{yw}}(f)^T \tag{9}$$

For example, the frequency response function from wind load vector to modal coordinate derivatives, $\boldsymbol{H_{\dot{q}w}}(f)$, can be computed as

$$\boldsymbol{H_{\dot{q}w}}(f) = \sqrt{-1}\ 2\pi f \left[-(2\pi f)^2\boldsymbol{M} + \sqrt{-1}\,2\pi f\boldsymbol{C_e} + \boldsymbol{K}\right]^{-1}\boldsymbol{L_{qw}} \tag{10}$$

The stationary RMS response of any quantity of interest is estimated in the frequency domain by integration of the corresponding one-sided PSD matrix, $\boldsymbol{S_{yy}}(f)$,

$$\mathrm{E}[\boldsymbol{y}\boldsymbol{y}^T] = \int_0^\infty \boldsymbol{S_{yy}}(f)df \tag{11}$$

Because equivalent damping parameters depend on rms deformation rates of the dampers and deformation rates of the dampers depend on the equivalent damping matrix where the equivalent damping parameters are assembled, the solution of the stationary response of the nonlinear model using statistical linearization requires an iterative procedure. Once convergence is achieved, mean square response of different quantities of interest can be computed, such as damper deformation-rates, floor accelerations at different locations, floor angular velocities, etc.

3.6 Equivalent modal damping ratios

Since the assembled equivalent damping matrix $\boldsymbol{C_e}$ is not classical, a state-space approach is followed to compute poles of the equivalent linear model by assembling the standard $\boldsymbol{A}$ matrix in state space. The equivalent natural frequencies and equivalent modal damping ratios are then computed from the eigenvalues of $\boldsymbol{A}$:

$$\mathbf{A} = \begin{bmatrix} \mathbf{O} & \mathbf{I} \\ -\mathbf{M}^{-1}\mathbf{K} & -\mathbf{M}^{-1}\mathbf{C_e} \end{bmatrix} \tag{12}$$

The equivalent natural frequencies and equivalent modal damping ratios are then computed from the eigenvalues of $\boldsymbol{A}$:

$$\boldsymbol{s} = \mathrm{eig}\,(A) \tag{13}$$

$$\omega_i = |s_i|\ ,\quad \xi = -\mathrm{Re}\,(s_i)/|s_i| \tag{14}$$

In the following sections equivalent damping ratios and building performance for the damper configurations are presented.

4 DYNAMIC PERFORMANCE COMPARISON FOR DAMPED TOWER

4.1 Modal Equivalent Damping and Performance

Using the statistical linearization method, a parametric analysis was performed modifying the damping constant (c_i) of the toggle dampers in the range where the optimum value that maximizes equivalent modal damping is located (starting from $20\ \mathrm{kN(s/m)^{\alpha}}$ to a maximum of $80\ \mathrm{kN(s/m)^{\alpha}}$) for different damper arrangements. The results of equivalent damping and

mean peak damper forces for each wind direction are shown in Figure 11 for configuration II only.

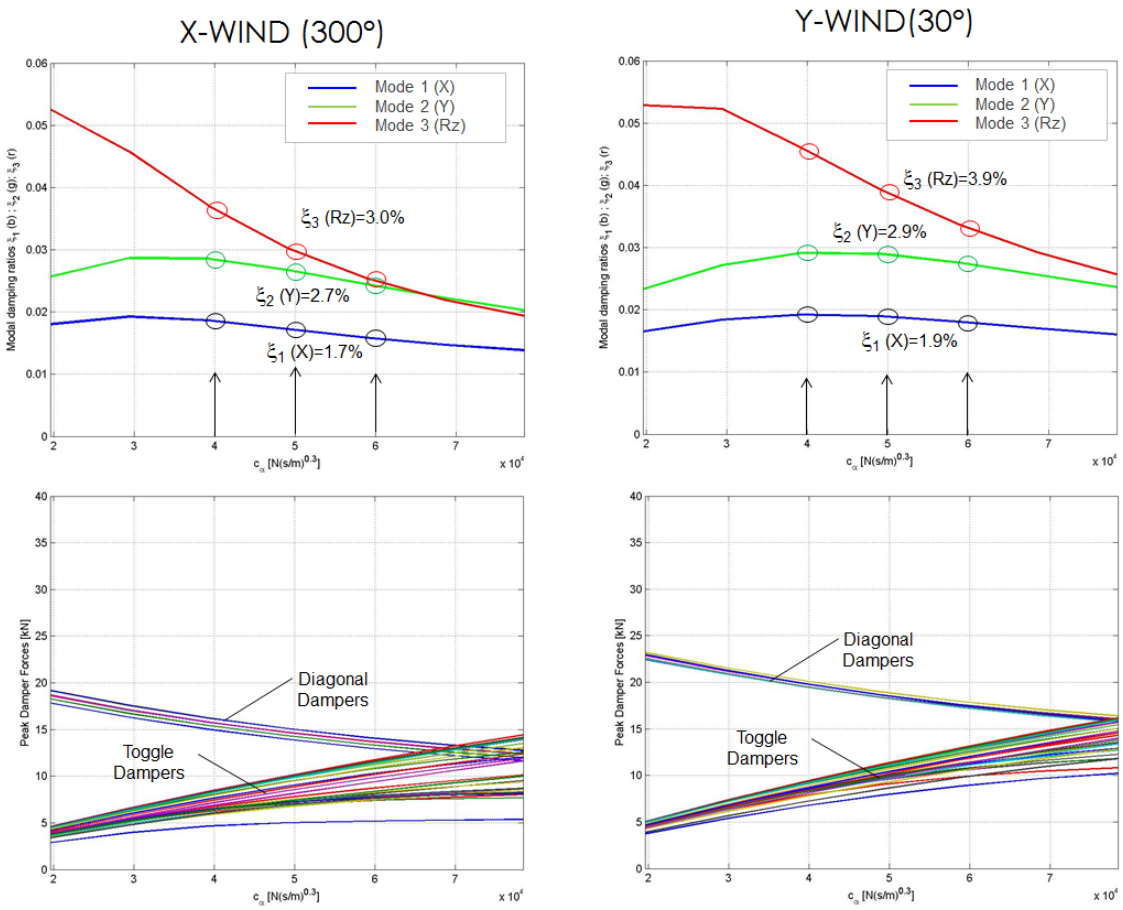

Figure 11. Arrangement II evaluation of equivalent modal damping and damper forces for different values of damping constant ($\boldsymbol{c_i = c}$) in toggle dampers.

Analogous results for other damper arrangements are not presented for brevity.

4.2 Performance evaluation

To be consistent with Windtech acceleration estimation reports where using only the first three main modes of the structure were considered, the estimated acceleration and floor angular velocity performance evaluation were computed considering the modal contribution of these modes only. Thus, even though the non-linear solution of the stochastic model is solved with the full reduced order model of 200 modes or coordinates, the results of this model, is calculated considering the contribution of the first three modal coordinates, only.

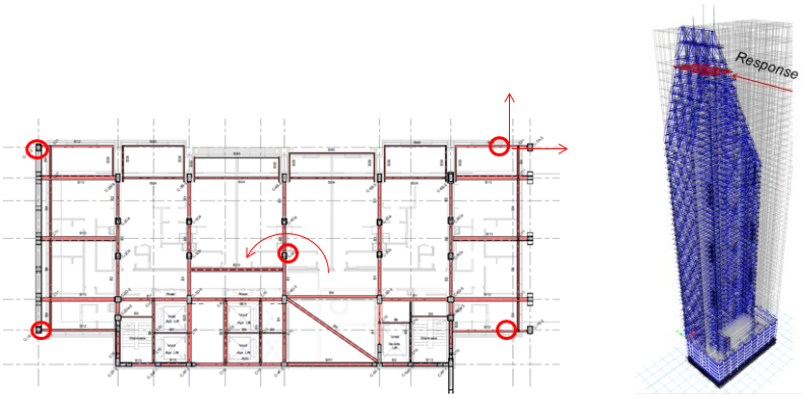

Figure 12. Points of each floor where total peak acceleration is evaluated in the building.

The following response parameters are obtained as part of the performance evaluation of the building:

- Total accelerations are estimated at corners of the building and floor CM.
- Peak X and Y components of accelerations are computed with Davenport's peak factor and RMS of each signal for a total duration of $T_w = 600\ s$ of stationary response.
- Total peak accelerations are computed combining orthogonal components using the approach proposed in Windtech's report.
- Peak angular velocities at each level are estimated using Davenport peak factor for $T_w = 600\ s$
- Other quantities: RMS and peak damper deformation and forces, and lateral dynamic displacements

To estimate mean peak responses from RMS responses, Davenport's peak factor is used:

$$g_f = \sqrt{2\ ln(\upsilon T_w)} + \frac{\gamma}{\sqrt{2\ ln(\upsilon T_w)}} \tag{15}$$

where $\gamma = 0.5772$ (Euler constant), $\upsilon =$ Mean zero-crossing rate and $T_w =$ stationary signal duration considered (seg.).

The mean zero-crossing rate for a given signal $y(t)$ is estimated assuming a Gaussian stationary process:

$$\upsilon_y = \frac{\sigma_{\dot{y}}}{2\pi\sigma_y} \tag{16}$$

As stated before, the duration of the stationary response was assumed as $T_w = 600\ s$ in the computation of the peak factor. To estimate mean peak damper forces, an approximation is developed valuing the nonlinear force-deformation rate relation of each damper at the mean peak deformation rate, $\dot{\Delta}$. The assessment of occupant comfort considers the total peak

acceleration (vector composition of X, Y and Z components). To estimate mean total peak acceleration at each point of interest the following formula is used

$$\hat{\sigma}_{a(x,y,x)} = \frac{\rho}{\sqrt{1+\rho^2}} \sqrt{\hat{\sigma}_{a(x)}{}^2 + \hat{\sigma}_{a(y)}{}^2} \tag{17}$$

where:

$\hat{\sigma}_{a(x)}$ $= g_{fx}\sigma_{a(x)}$: is the peak acceleration along X direction (same for Y direction)
ρ $= \max(\hat{\sigma}_{a(x)}, \hat{\sigma}_{a(y)})/\min(\hat{\sigma}_{a(x)}, \hat{\sigma}_{a(y)})$, when only 2 directions are considered
σ_{ax} : is the standard deviation acceleration along the X axis (same for Y direction)
g_{fx} : is the Davenport's peak factor calculated for σ_{ax}

Table 2. Arrangement II: equivalent damping and performance

		Model 36 VDs					
		36 VDs (14+8)VDs on GL 2 + (14)VDs on GL 6					
Wind Direction		300° (X)			30° (Y)		
Diagonal Disip. C constant	N (s/m)^α	526,000			526,000		
Diagonal Disip. α Constant	--	0.5			0.5		
Toggle Disip. C constant (GLs 2, 6, 4)	N (s/m)^α	40,000	**50,000**	60,000	40,000	**50,000**	60,000
Toggle Disip. α Constant (GLs 2, 6, 4)	--	0.3	**0.3**	0.3	0.3	**0.3**	0.3
Toggle Disip. C constant (GL D)	N (s/m)^α						
Toggle Disip. α Constant (GL D)	--						
Equivalent Damping X		0.019	**0.017**	0.016	0.019	**0.019**	0.018
Equivalent Damping Y		0.029	**0.027**	0.025	0.029	**0.029**	0.028
Equivalent Damping Rz		0.037	**0.030**	0.025	0.046	**0.039**	0.034
Mode 1 damped vibration freq. (X)	rad/s	1.290	**1.293**	1.295	1.285	**1.289**	1.291
Mode 1 damped vibration freq. (Y)	rad/s	1.422	**1.429**	1.434	1.414	**1.421**	1.428
Mode 1 damped vibration freq. (Rz)	rad/s	3.424	**3.441**	3.449	3.394	**3.419**	3.434
3 MODES RESPONSE							
Level 52 RMS Accel X. - Maximum in Level	millig	1.08	**1.14**	1.20	3.20	**3.20**	3.23
Level 52 RMS Accel Y. - Maximum in Level	millig	2.67	**2.73**	2.82	3.03	**3.04**	3.11
Level 52 Peak Total Accel. - Maximum in Level	millig	8.88	**9.10**	9.40	10.48	**10.48**	10.58
Level 52 Peak Angular velocity	milli rad/s	0.56	**0.58**	0.61	1.41	**1.43**	1.47
Diagonal Disip. Peak Force Envelope	kN	16.25	**15.12**	14.16	20.09	**18.97**	17.94
Toggle Disip. Peak Force Envelope (GLs 2, 6 and 4)	kN	8.36	**10.03**	11.59	9.28	**11.19**	12.96
Toggle Disip. Peak Force Envelope (GL D)	kN						

Damper capacity increase Wind X

Damper capacity increase Wind Y

Although computation of mean peak acceleration and mean peak floor angular velocity are done at all floors, level L52 performance is used for comparison. In general terms, both peak total acceleration and peak angular velocities are smaller at lower levels. Table 2 presents the performance estimation for OCC for wind in X and Y direction for the structure with damper arrangement II.

4.3 Performance for other damper configurations

Table 3 presents a summary of performance estimated for the tower with TMD and damper arrangement VI.

Table 3. Arrangement VI: equivalent damping and performance

		Model 36 VDs+TMD - 3Modes	
		36VDs + TMD (14+8)VDs on GL 2 + (14)VDs on GL 6 + 150Ton TMD	
Wind Direction		300° (X)	30° (Y)
Diagonal Disip. C constant	N (s/m)^α	526,000	526,000
Diagonal Disip. α Constant	--	0.5	0.5
Toggle Disip. C constant (GLs 2, 6, 4)	N (s/m)^α	50,000	50,000
Toggle Disip. α Constant (GLs 2, 6, 4)	--	0.3	0.3
Toggle Disip. C constant (GL D)	N (s/m)^α		
Toggle Disip. α Constant (GL D)	--		
Equivalent Damping X		0.0484 - 0.0590	0.0487 - 0.0595
Equivalent Damping Y		0.0376 - 0.0456	0.0393 - 0.0489
Equivalent Damping Rz		0.0239	0.0317
Mode 1 damped vibration freq. (X)	rad/s	1.1985 - 1.2752	1.1966 - 1.2725
Mode 1 damped vibration freq. (Y)	rad/s	1.3445 - 1.5035	1.3428 - 1.5003
Mode 1 damped vibration freq. (Rz)	rad/s	3.453	3.44
3 MODES RESPONSE			
Level 52 RMS Accel X. - Maximum in Level	millig	0.71	2.15
Level 52 RMS Accel Y. - Maximum in Level	millig	1.83	1.95
Level 52 Peak Total Accel. - Maximum in Level	millig	6.12	7.15
Level 52 Peak Angular velocity	milli rad/s	0.47	1.06

Table 4 shows the equivalent modal damping ratios for the first three modes of vibration of the equivalent lineal model for different optimized damper arrangements.

Table 4. Summary of equivalent modal damping ratios obtained for damper configurations

Damper Arrangement	Equivalent modal damping ratio (ξ)					
	X Wind Direction			Y Wind Direction		
	Mode 1 (X)	Mode 2 (Y)	Mode 3 (Rz)	Mode 1 (X)	Mode 2 (Y)	Mode 3 (Rz)
II. 36 VDs	1.7%	2.7%	3.0%	1.9%	2.9%	3.9%
III. 60 VDs	2.0%	3.0%	3.3%	2.2%	3.3%	4.4%
IV. 54 VDs	1.7%	2.5%	2.7%	2.0%	2.8%	3.6%
V. 73 VDs	2.3%	3.0%	3.2%	2.8%	3.3%	4.1%
VI. 36VDs + TMD	4.8%–5.9%	3.8%–4.6%	2.4%	4.9%–5.9%	3.9%–4.9%	3.2%

Figures 13 and 14 present a summary of the estimated peak total accelerations and peak rotational velocities at level 52 of the building for all damping configurations studied.

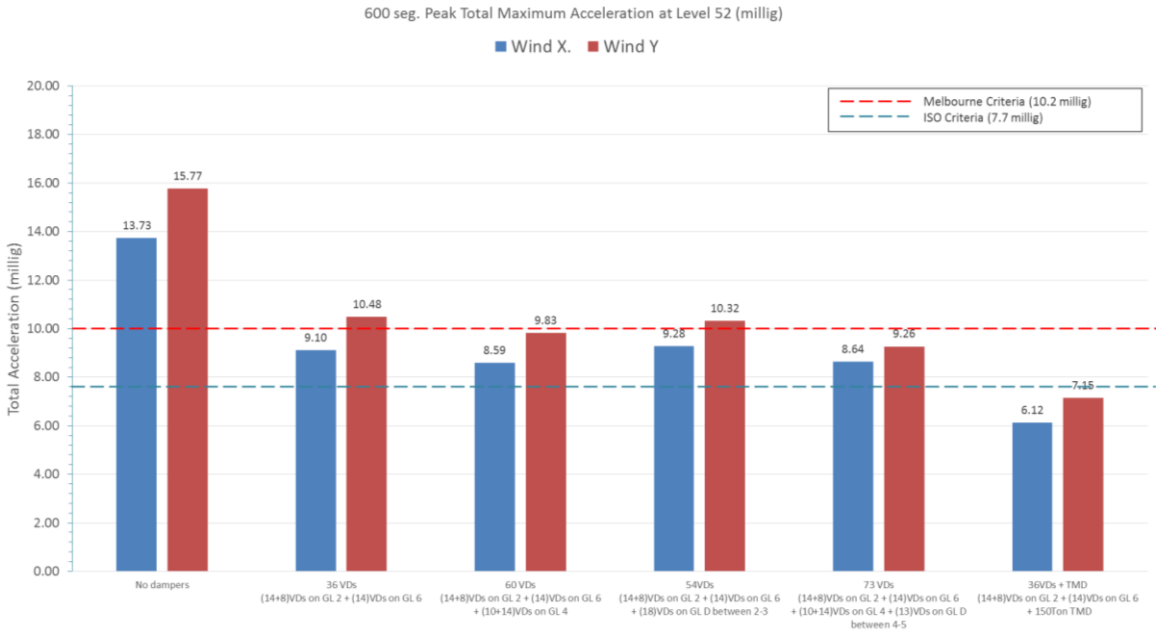

Figure 13. Summary of maximum peak accelerations at Level 52 obtained for damper configurations

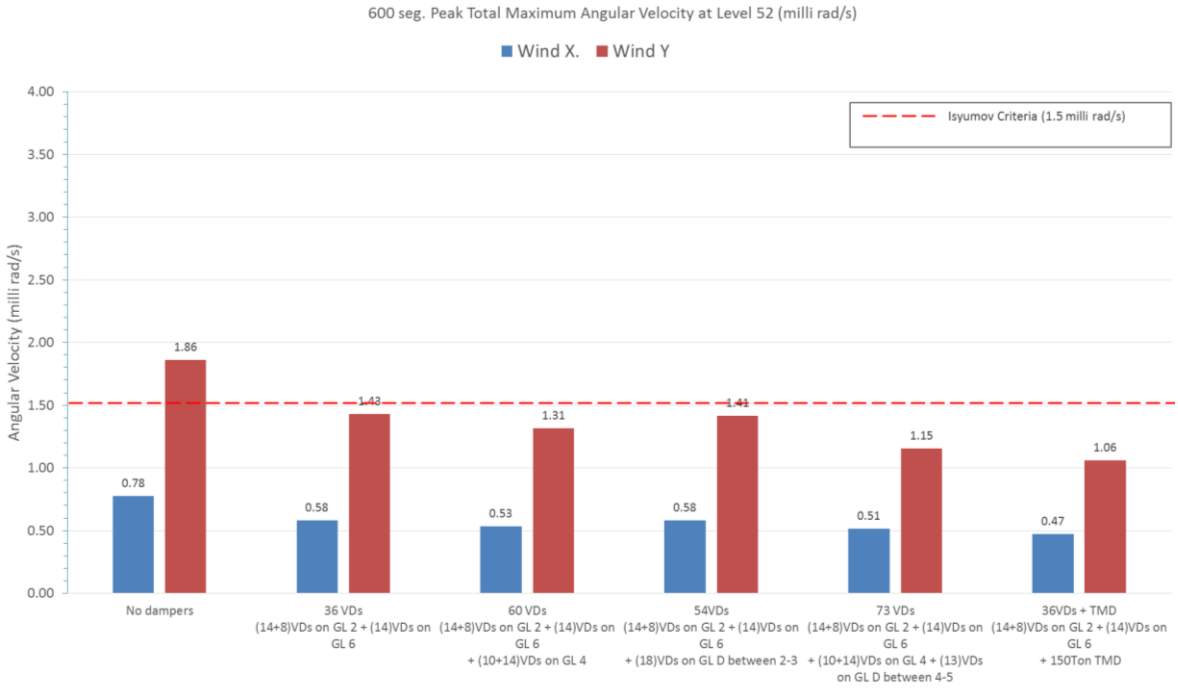

Figure 14. Summary of maximum peak accelerations at Level 52 obtained for damper configurations

The following conclusions arise from the results obtained of the probabilistic analysis for X and Y wind directions:

- Arrangement I (all VDs on straight braces) is not suitable for a proper functioning of energy dissipation devices (very small RMS displacements at all levels)

- Arrangement II (36VDs on GLs 2 and 6) generates significant acceleration reductions almost reaching Melbourne criterion. Angular velocities achieve the acceptance criteria.
- Arrangements III and IV (60 and 54 VDs) require at least 50% more dampers than arrangement 2, and performance remains almost unaffected. The Toggle angle considered for dampers on GL D (~20°) reduces the amplification from about 4,5 to ~1.35. This angle was selected due to architectural constraints.
- Arrangement V (73VDs on GLs 2, 4, 6 and D) yields damping ratios close to the target, and reaches the performance criteria. However, the dampers located on GL D between GLs 4 and 5 are not suitable for the architectural design of the building.

Thus, the incorporation of a TMD system could be required to achieve performance objectives, in which case the results are:

- The 150 ton TMD introduces an additional reduction that reaches the ISO criteria for acceleration peak values.
- Different TMD frequencies were considered for each direction of the building (X and Y).
- The reduction of rotational velocity is presumed to be achieved by controlling the X vibration mode of the building, which exhibits significant floor rotations.

4.4 Artificial wind force signals for time-domain structural simulation

For validation purposes, a complete structural model (ETABS) was analyzed considering nonlinear constitutive relationships of proposed viscous damping devices, and a set of time history wind load signals compatible with the stochastic wind model used in reduced order analyses. The purpose of generating random samples of wind forces and moments compatible with the developed wind model, was to validate peak damper forces and deformations, peak total acceleration and peak angular velocity reductions at Level 52 using numerical simulation in the nonlinear models. In the preliminary design stage, few artificial signals were run for each damping strategy considered. In the following detailed engineering phase, artificial compatible wind-force signals can be used for further performance verification of the final design configuration using Monte Carlo simulation.

Along the wind, across the wind and torsional moment sample signals were generated for each floor of the building to be applied as specified loads in the ETABS model. Using the cross power spectral density matrix of along the wind forces and across the wind forces for each level, and the Cholesky decomposition of the cross power spectral density matrices, random force samples were simulated using Shinozuka´s method of superposition of random harmonic signals. Signals were generated using a sampling time of 0.1 seconds. Wind forces were applied in the center of gravity of exposed surfaces at each floor for the along the wind and across the wind directions. An additional independent free torsional moment vector (Z direction) was created to account for random eccentricity, including coherence in height and adjusted with torsional moments measured in wind tunnel tests by Windtech.

Figure 15 shows the PSDs of the theoretical model (green line) for lift force (across the wind load) at L51 and L11 compared with the PSD estimated from the generated samples (red lines).

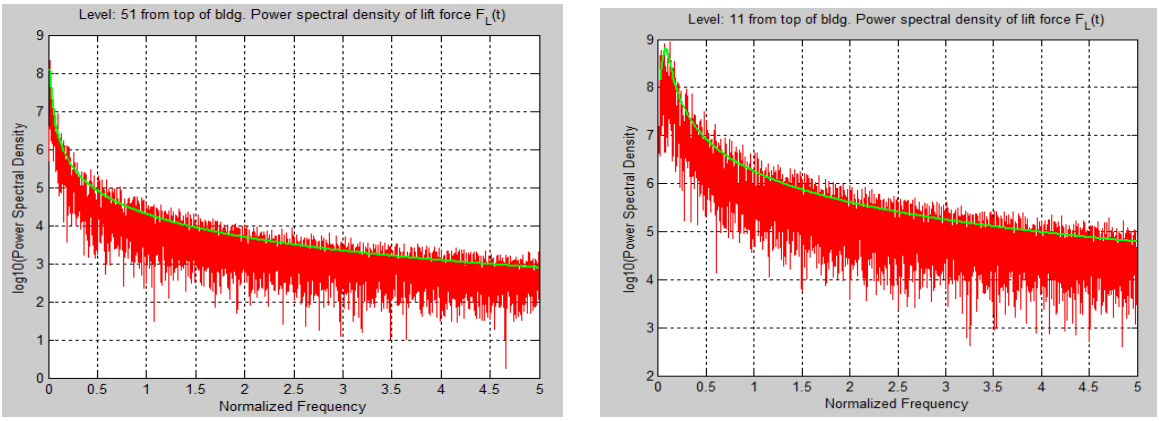

Figure 15. PSD comparison in $\log_{10}$ scale of theoretical forces (green) and generated signals (red), at level L51 (left) and L11 (right)

4.5 Performance Validation by numerical integration with simulated wind force signals

The purpose of performing nonlinear time-history analyses was to perform a separated validation of the probabilistic methodology. Thus, the following objectives and limitations are stated:

- Time-history analyses are for validation purposes only.
- The valid results, in terms of equivalent damping and all other performance outputs, are the obtained from the probabilistic analyses.
- Time-history artificial wind force signals were generated to represent, as close as possible, the theoretical stochastic wind model calibrated to the wind tunnel information
- As wind loading is a random process, several time-history wind signals should be analyzed in order to obtain more accurate results. Only 2 different signals for each direction (X and Y) were calculated for the preliminary evaluation stage. The performance verification of the final design configuration is evaluated using several wind signals.
- Some differences may arise between probabilistic and time-history results, but general behavior and order of magnitude of the response parameters should be consistent.

Each story of the building structural model is loaded with a unique set of 3 load time-history signals. Thus, each analysis, for each wind direction requires 147 signals of wind loading vector $\mathrm{w(t)}$, $(3\,\mathrm{signals/story} \times 49\mathrm{stories} = 147\ \mathrm{signals})$. The response is integrated in 360 seconds time-history signals (same as input loads).

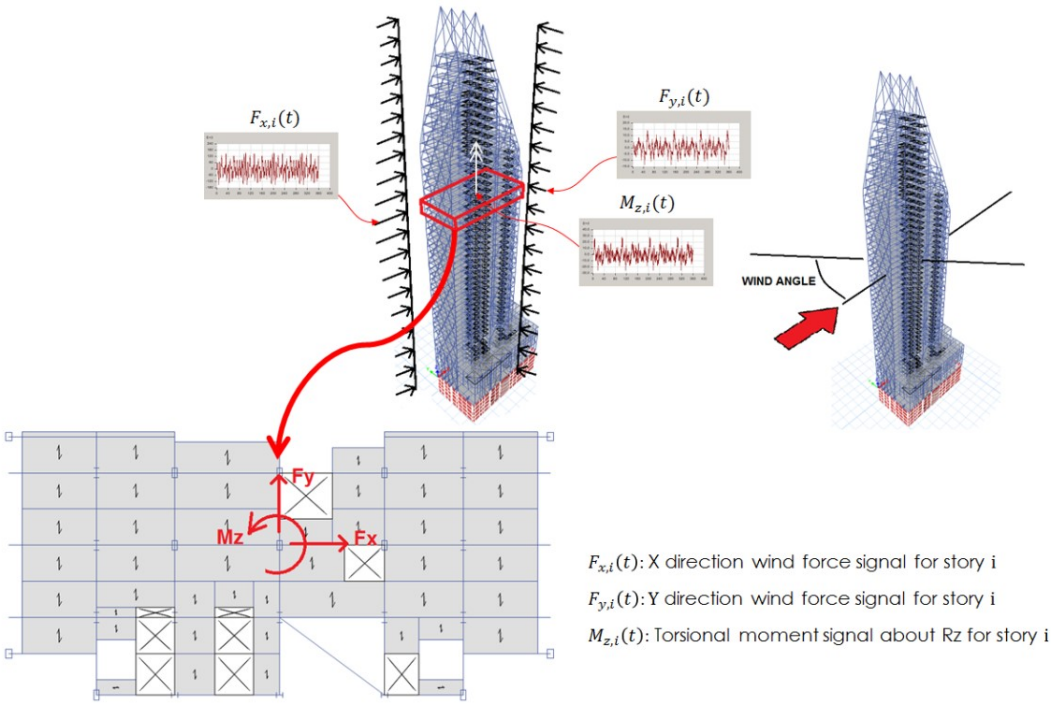

Figure 16. Loading of time-history load signals

As peak values must represent 600 seconds (for OCC) of exposure to wind loading, peak values are calculated as follows:

- The first 100 seconds of the output signals are discarded, as those contain the transient response before the structure reaches steady-state regime (analysis starts from zero initial condition).
- RMS is calculated for the remaining 260 seconds.
- Peak factor (Davenport formula) is calculated for the response signal, for 600 seconds, and applied to the RMS value of the 260 seconds output signal.
- If directional composition is required, the peak values of X and Y directions are composed following the same procedure as for probabilistic results.

The validation of probabilistic analyses was performed only for Arrangement II (36 VDs) and Arrangement VI (36 VDs + TMD), because these are the alternatives showing better performance and smaller number of damping devices. It is important to notice that time history results in this case are calculated including the participation of all modal coordinates, not only the first three ones. The estimated performance computed with the contribution of all modal coordinates is shown in Figure 17. Responses are calculated at the corner points and CM of all stories. Floor accelerations in *X* and *Y* direction at the center of mass at level L52 are depicted in Figure 17.

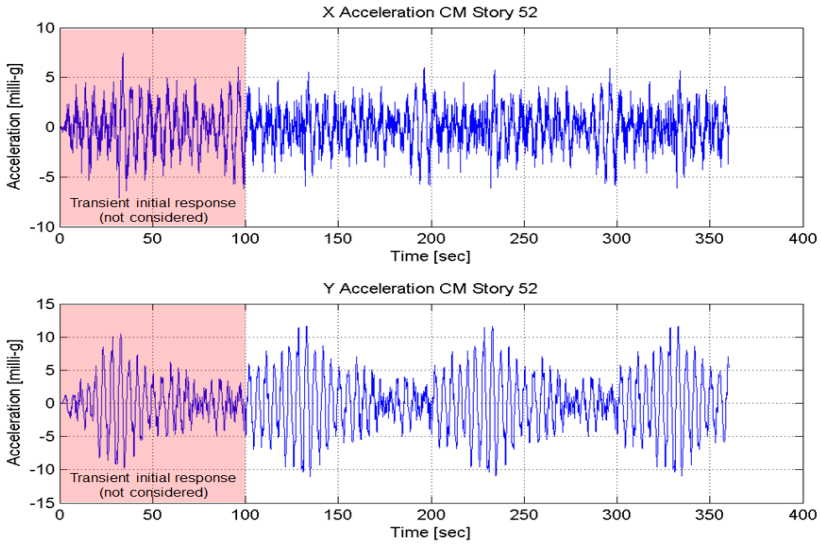

Figure 17. Acceleration time history result at level 52 for Wind acting in direction Y
(Direct results of Arrangement II for all mode contribution, not scaled by peak factor)

Figure 18 presents the force-displacement hysteresis of a damper connected by a toggle brace. The low exponent ($\alpha = 0.3$) explains the low sensitivity of peak force to cyclic deformation amplitude of the damper.

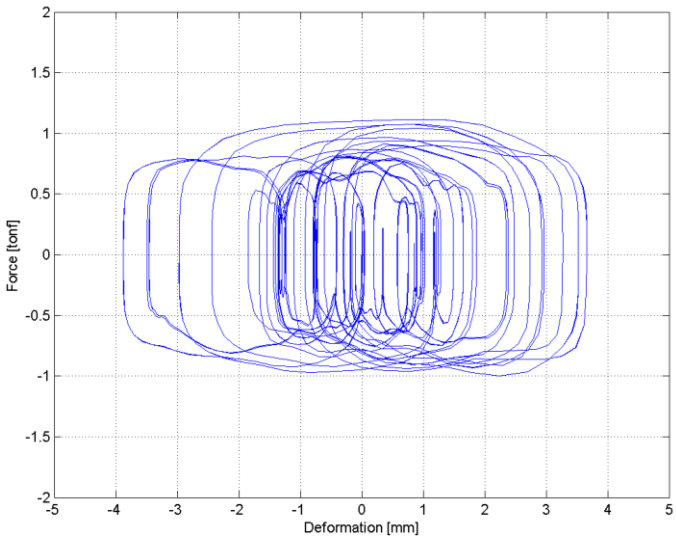

Figure 18. Typical force-displacement hysteresis obtained in toggle braces for wind acting in Y direction.

Figure 19 presents the results obtained for the comparison between probabilistic and time history analyses. In all cases the differences between both models are less than 10%, which is considered reasonable for results coming from totally different analysis approaches and considering that mean peak accelerations have been estimated with only 2 artificial signals.

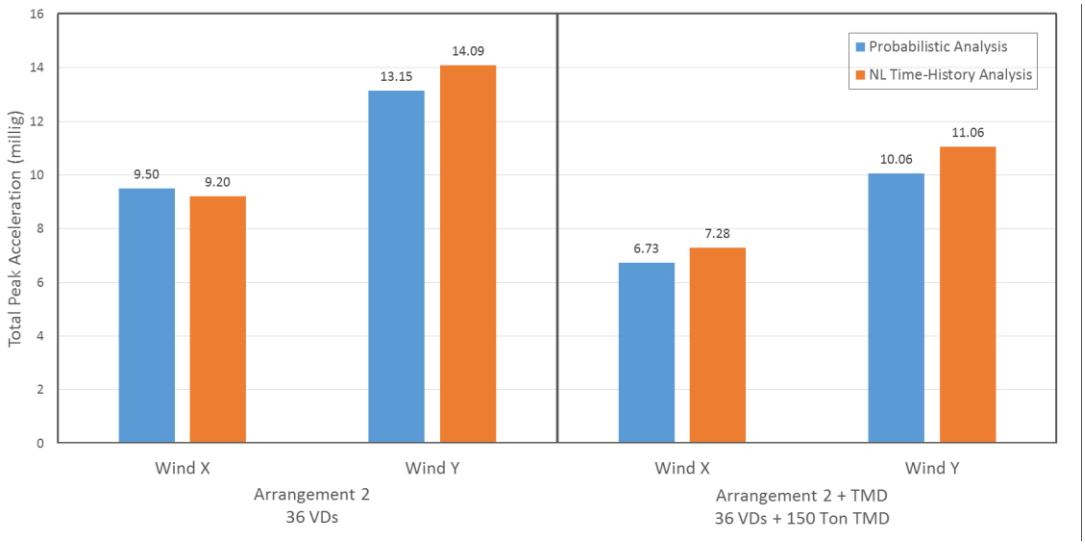

Figure 19. Comparison between Probabilistic and Nonlinear Time-history Analysis

4.6 Damper performance for extreme wind

The results for the analyses performed for wind ultimate (1.000 yr. return period) and earthquake conditions are presented in this section for configuration II. The results were computed to complete the design of the dampers and diagonal connectors (peak forces, peak deformations and total energy dissipation are the main variables of interest for design defined by extreme wind and earthquake conditions).

Table 5. Summary Response parameters for 1.000 yr. return period wind load
Calculated as mean value of 10 analyses per wind direction

Response Parameter	Units	Wind Direction	
		X	Y
Response at level 52			
Maximum Peak Acceleration	milli-g	44.48	31.05
Maximum Peak Rotational Velocity	milli rad/s	4.89	5.67
Toggle Dampers			
Maximum Peak Velocity	mm/s	61.30	39.42
Maximum Peak Force	kN	21.47	18.88
Maximum Peak for Wind Dynamic Displacement	mm	113.74	98.54
Maximum Displacement for Wind Static Component	mm	54.45	54.45
Maximum Displacement for Dead Loads	mm	41.02	41.02
Maximum Displacement for Live Loads	mm	12.09	12.09
Diagonal Dampers			
Maximum Peak Velocity	mm/s	11.70	7.84
Maximum Peak Force	kN	56.27	46.29
Maximum Peak for Wind Dynamic Displacement	mm	21.87	18.68
Maximum Displacement for Wind Static Component	mm	10.27	10.27
Maximum Displacement for Dead Loads	mm	9.65	9.65
Maximum Displacement for Live Loads	mm	2.70	2.70

The mean values of estimated demands are presented in Table 5. The results shown in this section are computed by numerical integration of the full ETABS® model. The displacements presented are only the dynamic response component of the building to wind loading. The

static deformations due to static component of wind actions and other static loads affecting the building (e.g. dead and live loads) are also shown separately in the table.

Figures 20, 21, 22 and 23 present estimated damper forces and deformations obtained for the dampers on Gridline 2 of the building. The minimum (blue-left x mark), mean (black-center o mark) and maximum (blue-right x mark) values of the 10 analyses performed for each wind direction are illustrated in each graph.

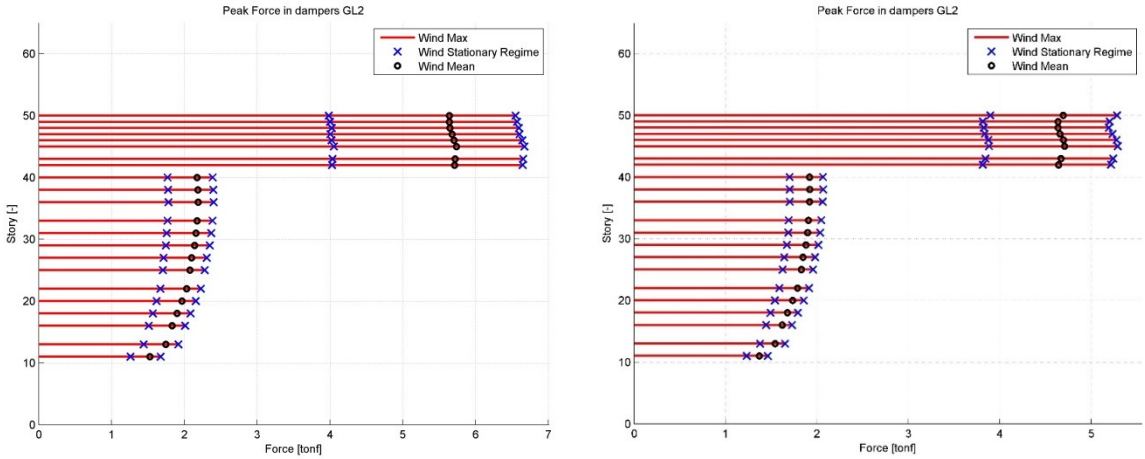

Figure 20. Gridline 2 - Maximum peak damper forces at the different stories of the building for wind X (left) and wind Y (right)

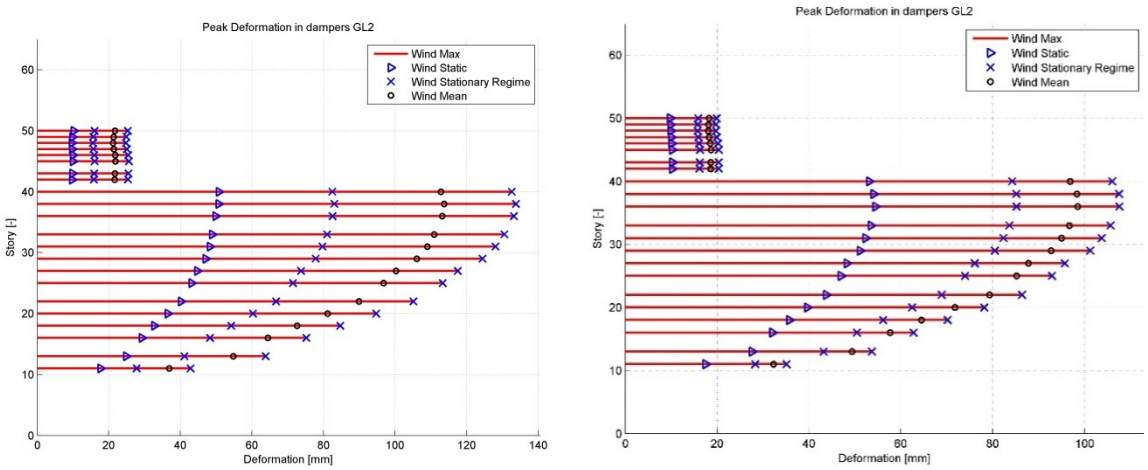

Figure 21. Gridline 2 - Maximum peak damper deformations at the different stories of the building for wind X (left) and wind Y (right)

The same results are presented next for the dampers on gridline 6 of the building. Again, the minimum (blue-left x mark), mean (black-center o mark) and maximum (blue-right x mark) values of the 10 analyses performed for each wind direction are illustrated in each graph.

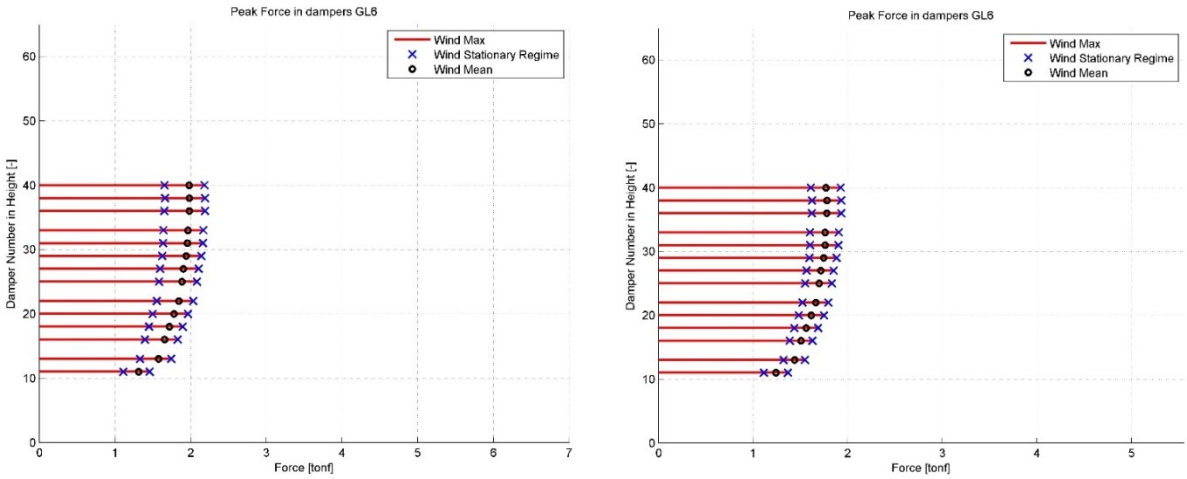

Figure 22. Gridline 6 - Maximum peak damper forces at the different stories of the building for wind X (left) and wind Y (right)

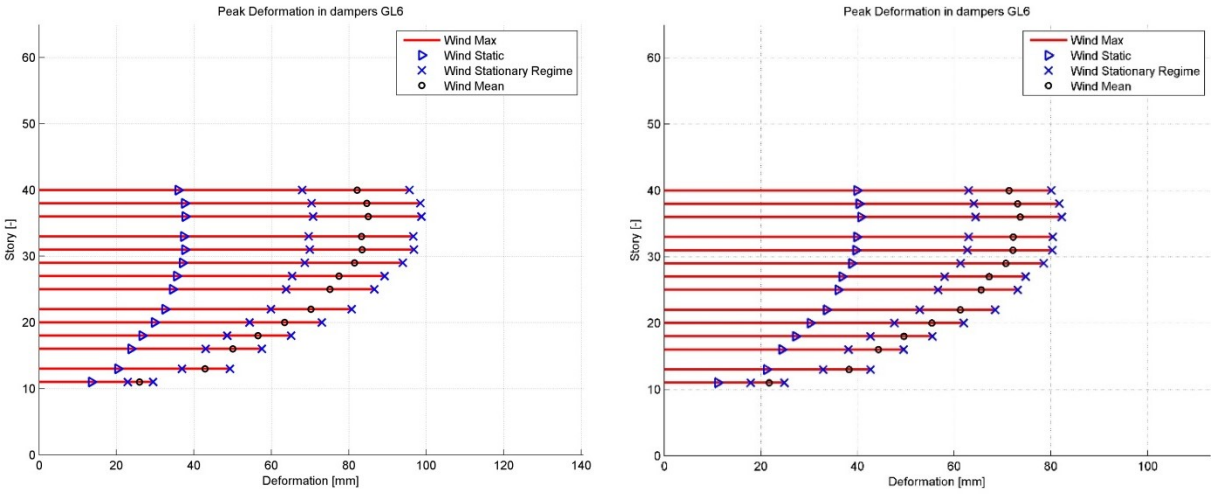

Figure 23. Gridline 6 - Maximum peak damper deformations at the different stories of the building for wind X (left) and wind Y (right)

4.7 Damper performance for extreme earthquake conditions

Dampers and their supporting braces must remain functional after the maximum credible earthquake, which according to New Zealand seismic design code (NZS 1170.5, 2004) is represented by the 2.500 year return period earthquake. The parameters defining this seismic design spectrum for the building location are:

Site subsoil class: C
Hazard factor: Z = 0.13
Return Period Factor: R = 1.8 (2500 return period earthquake).
Near fault distance: D = 50 (km).

To estimate peak damper forces and deformations for extreme earthquake scenarios, artificial seismic acceleration signals were created based on real seismic records (El Centro, Century City, and Lucerne) modified to be compatible with this seismic design spectrum. The response spectra for the modified El Centro and Century City Los Angeles signals are shown in the following figure.

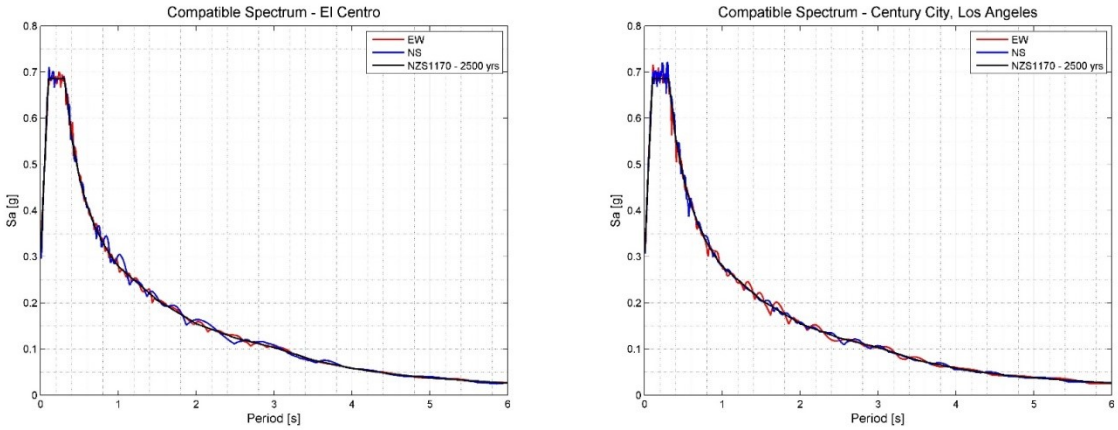

Figure 24. Response spectrum for El Centro earthquake record and Century City (LA) earthquake records adjusted to the 2.500 return period spectrum (NZS 1170)

Table 6. Response parameters for 2.500 yr. return period earthquake
Calculated as envelope value of 3 seismic analysis

Response Parameter	Units	SEISMIC RECORD		
		EL CENTRO	CENTURY CITY, LA	LUCERNE
Toggle Dampers				
Maximum Velocity	mm/s	677.11	730.23	668.60
Maximum Force	kN	44.47	45.49	44.30
Maximum Seismic Displacement	mm	138.68	155.21	111.61
Maximum Displacement for Dead Loads	mm	41.02	41.02	41.02
Maximum Displacement for Live Loads	mm	12.09	12.09	12.09
Diagonal Dampers				
Maximum Velocity	mm/s	335.40	159.89	177.64
Maximum Force	kN	304.01	209.90	221.24
Maximum Seismic Displacement	mm	28.29	23.10	24.78
Maximum Displacement for Dead Loads	mm	9.65	9.65	9.65
Maximum Displacement for Live Loads	mm	2.70	2.70	2.70

Peak damper forces and deformations for extreme earthquake signals obtained for the dampers on gridlines 2 and 6 (configuration II) are shown in Table 6 and Figure 24. The minimum (blue-left x mark), mean (black-center o mark) and maximum (blue-right x mark) values obtained for three seismic analyses corresponding to artificial ground-acceleration signals are illustrated in each graph.

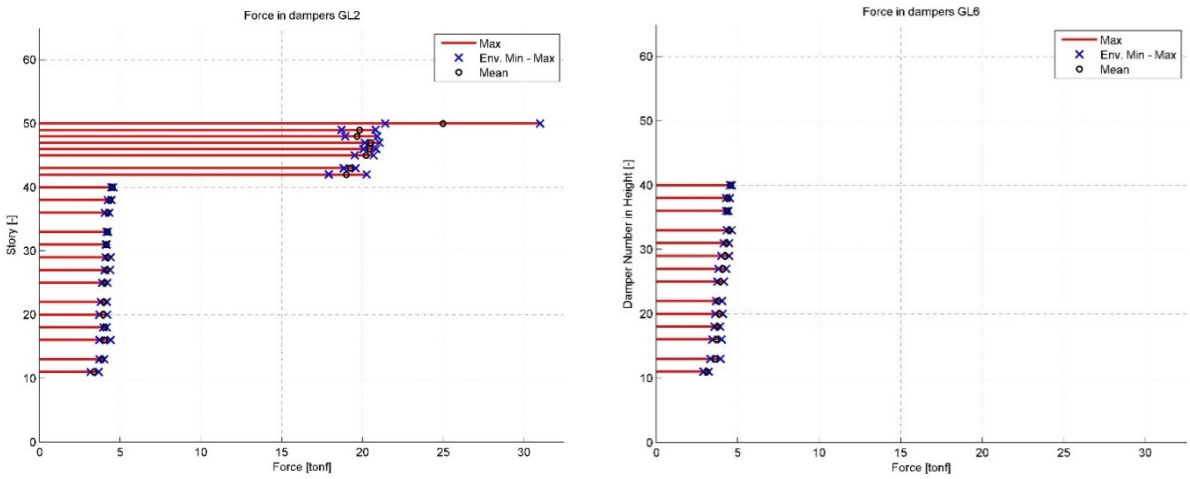

Figure 24. Maximum peak damper forces at the different stories of the building for Gridline 2 (left) and Gridline 6 (right)

Large peak damper force demand on dampers located on diagonal braces above level 40 for earthquake design condition, determined the consideration of new damper configurations (II-b and VI-b) eliminating those dampers from configurations II and VI, to reduce bracing cost. Expected OCC wind performance for these modified damper configuration were recomputed providing minor peak total floor acceleration increases with respect to configurations II and VI. Estimated performances of modified configurations II-b and VI-b are not shown for brevity.

5 CONCLUSIONS

The damper-configuration selection process and main performance results obtained for a steel frame subjected to wind events have been described. Occupant comfort improvement with minor structural modifications was the design objective formulated by the structural engineer of the analyzed 180 m height tower to be built in Auckland, New Zealand. Several damper configurations, including a supplemental TMD, were studied. The main steps followed for damper configuration selection have been briefly described.

The use of nonlinear viscous energy dissipating devices to reduce peak floor accelerations proved to be a sound strategy to improve building performance for low wind intensity events, minimizing costs of structural connectors to the main structural system. Equivalent damping ratios in the first three modes of vibration and expected mean peak total floor accelerations were estimated for several damper locations varying damper parameters to select optimum parameters of each damper distribution considered. Floor acceleration and peak floor angular velocities achieved with supplemental viscous dampers and a tuned mass damper were evaluated to comply with occupant performance standards.

The estimation of mean peak floor accelerations to random wind forces and the design procedure of supplemental nonlinear viscous dampers in one-year recurrence wind events and extreme wind and earthquake events have been reported. A stochastic wind load model that estimates drag, lift and torsional moments at each story as random stationary processes was developed for damper configuration performance estimation. Wind tunnel results and

computational fluid dynamic analyses were used to fine-tune the stochastic load models before performance estimation. Reduced-order structural models of the tower were developed using Ritz-mode parameters computing using an ETABS® structural model developed by the structural engineering consulting firm in charge of the project to estimate the frequency response function from floor loadings to floor accelerations at corners points of the buildings and other outputs of interest. The statistical linearization method was used to estimate the performance of the buildings with non-linear viscous dampers installed in different configurations. Monte Carlo simulation of wind loading was employed to validate estimated performance in the nonlinear model for selected configurations using direct nonlinear integration of the equations of motion of the building model with nonlinear viscous devices.

ACKNOWLEDGEMENTS

We specially acknowledge the valuable contribution and interaction with Mott MacDonald and Windtech Consultants for inviting us for this damper-design challenge. We thank Carlos Sacco and Esteban Gonzalez for their contribution in CFD analyses for this project.

REFERENCES

ISO 10137, Bases for design of structures - Serviceability of buildings and walkways against vibrations, 2007.

Mott MacDonald, *Structural Engineering Design Development Report*, Mott MacDonald, December 2015.

Windtech Consultants, *Wind-Induced Structural Loads and Building Motion Study* (WC470-02F02(Rev1)-BB Report, Windtech Consultants Pty Ltd, September 12, 2016.

Kareem, A., Dynamic Response of High-Rise Building to Stochastic Wind Loads, *Journal of Wind Engineering and Industrial Aerodynamics*, 41-44, 1101-1112, 1992.

Y. Tamura and A. Kareem, *Advanced Structural Wind Engineering*, editors, Springer, Japan, 2013.

AS/NZS 1170.2, *Structural design actions Part 2: Wind Actions*, 2011.

NZS 1170.5, Supplement 1, *Structural design actions Part 5: Earthquake actions* – New Zealand, 2004.

Melbourne W.H. and Cheung, J.C., Designing for serviceable accelerations in tall buildings, *Proceedings of the Fourth International Conference on Tall Buildings*, Hong Kong and Shangai, China, 148-155, 1988

Isumov N., Criteria for acceptable wind-induced motions o tall buildings, *International Conference on Tall Buildings*, 401-411, 1993.